# Numerical Study of the Impacts of Urban Expansion on Meiyu Precipitation over Eastern China

MA Xinye (马新野) and ZHANG Yaocun* (张耀存)

*School of Atmospheric Sciences, Nanjing University, Nanjing* 210023

(Received May 21, 2014; in final form October 13, 2014)

**ABSTRACT**

The Yangtze River Delta (YRD) has experienced significant urban expansion in recent years, while the Meiyu belt of China has demonstrated a decadal northward shifting trend. Thus, it is of interest to assess how urban expansion affects Meiyu precipitation and hopefully to reveal the underlying physical mechanisms involved. In this study, the urban extents over the YRD in 2001 and 2010 are derived based on land use/land cover (LULC) category data and nighttime light image data. Two parallel groups of 10-summer (2001–2010) numerical simulations are carried out with the urban extents over the YRD in 2001 and 2010, respectively. The results show that the urban expansion in the YRD tends to result in increased (decreased) Meiyu precipitation over the Huaihe River (Yangtze River) basin with intensities of 0.2–1.2 mm day$^{-1}$. Further analysis indicates that the spatiotemporal pattern of the Meiyu precipitation change induced by the urban expansion resembles the third empirical orthogonal function (EOF) mode of the observed Meiyu precipitation. Analyses of the possible underlying physical mechanisms reveal that urban expansion in the YRD leads to changes in the surface energy balance and warming (cooling) of tropospheric (stratospheric) air temperature over eastern China. Anomalous upward (downward) motion and moisture convergence (divergence) over the Huaihe River (Yangtze River) basin occur, corresponding to the increases (decreases) of the Meiyu precipitation over the Huaihe River (Yangtze River) basin.

**Key words:** urban expansion, MODIS (Moderate-resolution Imaging Spectroradiometer) LULC category data, Yangtze River Delta, Meiyu precipitation, trend

**Citation:** Ma Xinye and Zhang Yaocun, 2015: Numerical study of the impacts of urban expansion on Meiyu precipitation over eastern China. *J. Meteor. Res.*, **29**(2), 237–256, doi: 10.1007/s13351-015-4063-5.

## 1. Introduction

Urbanization, as an extreme case in terms of land use/land cover (LULC) change, modifies albedo, emissivity, and thermal conductivity of the land surface. Urban regions have a larger heat-storage capacity, Bowen ratio, and an increased surface roughness in comparison with rural regions (Oke, 1982). These differences lead to changes in the exchange of energy, momentum, and moisture, ultimately affecting the regional climate (Charney et al., 1977; Chase et al., 1996; Stohlgren et al., 1998; Eastman et al., 2001; Foley et al., 2005; Lin et al., 2007; Feng et al., 2012). Therefore, urbanization and climate change are becoming increasingly interconnected (Seto and Shepherd, 2009).

The variation in precipitation is an important indicator for climate change, so proper assessments of the urban environmental impacts on precipitation are becoming increasingly important (Shepherd, 2005). In recent years, some researchers have used observational data and numerical models to study the local impacts of urbanization on precipitation. For instance, Shepherd et al. (2002) found that the monthly mean rainfall could increase by 28% over the region 30–60 km downwind of a metropolis. Similarly, Mote et al. (2007) pointed out that areas to western Atlanta receive 30% less rainfall than eastern Atlanta as a result of urbanization effects. Also, Chen et al. (2007) found that urbanization in Taipei could be a contributor to the 67% increase in the frequency of afternoon thunderstorms and the 77% increase in rainfall. Zhang et

Supported by the National Basic Research and Development (973) Program of China (2011CB952002 and 2010CB428504).
*Corresponding author: yczhang@nju.edu.cn.

al. (2009) suggested that the rapid urban expansion that has taken place in Beijing since 1981 is statistically correlated to a summer rainfall reduction in the northeastern areas of the city from 1981 to 2005. By analyzing model results, Shepherd et al. (2010) found that simulations that included a representation of urban areas, in comparison to those without, produced more cumulative rainfall over the region to the west-northwest of Houston. Based on the results from 10-summer and 1-km resolution WRF (Weather Research and Forecasting) nested model simulations for the period 2000–2009, Yang et al. (2012) found a larger precipitation frequency over urban areas in Nanjing (eastern China) and a significant enhancement of precipitation in the downwind region of the city in the afternoon.

However, all of the above-mentioned studies focused on the urbanization effects on local precipitation, while the impacts of urbanization on precipitation on regional or larger scales have received far less attention. In fact, the urbanization effects on precipitation depend on the climate regime and geographical locations of cities (Zhang et al., 2009). Some studies have suggested that urbanization has significant effects on atmospheric circulation, convection, and regional precipitation amounts and patterns. For example, Kishtawal et al. (2010) found that the frequency of heavy rainfall has been increasing in urban regions of India during the monsoon season. Meanwhile, by employing nested high-resolution WRF modeling, Wang et al. (2012) found that urbanization reduces the rainfall amount over urban areas, mainly in summer, and changes the regional precipitation pattern to a certain extent. Also, by simulating a summertime rainstorm process with/without the presence of urban areas in the Yangtze River Delta (YRD), Wan et al. (2013) found that the increases in precipitation mainly occur downwind of the city belt, and that the increases and decreases in precipitation are represented as adjacent belts to the main precipitation belt.

The YRD economic belt is one of the most urbanized and developed areas in China. Several studies have found that urbanization over the YRD has led to increases in local and regional surface air temperature (Du et al., 2007; Yang et al., 2011; Wu and Yang, 2013) and modifications to regional-scale precipitation (Zhang et al., 2010; Sang et al., 2013). In recent years, the YRD has maintained its rapid urban expansion (Zhang et al., 2010). However, few studies have been carried out looking at the impacts of the urban expansion of this region on regional-scale precipitation.

Meiyu is a unique rainy season over East Asia that takes place during the northward progression of the East Asian summer monsoon (EASM) from late spring to mid summer (Si et al., 2009). In China, Meiyu is a dominant climate phenomenon over the Yangtze-Huaihe River basin between mid June and mid July, and has been intensively studied (Gong and Ho, 2002; Wei and Xie, 2005; Zong et al., 2006; Ding et al., 2007; Bueh et al., 2008; Huang et al., 2011; Wu and Zhang, 2012). Recent studies show an increasing trend of Meiyu precipitation over the Huaihe River basin and a relative decreasing trend over the Yangtze River basin since the late 1990s. For instance, severe floods occurred over the Huaihe River basin in 2003, 2005, and 2007 (Zhao et al., 2007; Zhang et al., 2008), suggesting that the great east-west thermal gradient associated with vegetation biophysical processes may contribute to the abrupt northward jump of the Meiyu belt (Xue et al., 2004). Also, Si et al. (2009) found that the Meiyu belt of China experienced a decadal northward shift in the late 1990s, as a result of a distinctive tropospheric warming and stratospheric cooling trend in the midlatitudes over East Asia. In addition, Liu et al. (2012) suggested that a strengthening of the EASM since the 1990s, linked to the interdecadal change of land-sea thermal contrast, has led to the northward-moving rainbands and excessive rainfall over the Huaihe River basin.

Against this background of climate change, urban expansion in the YRD, which is located in the Yangtze-Huaihe River basin, may also contribute to changes in precipitation during the Meiyu season. Therefore, the primary goal of the present reported research was to identify and quantify the impacts of urban expansion in the YRD on precipitation and atmospheric circulation during the Meiyu period, and investigate the possible underlying physical mechanisms.

The remainder of the paper is organized as follows. A description of the data and methods used in the study is given in Section 2. In Section 3, the model and numerical experiment designs are described. A validation of the model results and analyses of the impacts of urban expansion on Meiyu precipitation, surface energy balance, and circulation are presented in Section 4. Concluding remarks are provided in Section 5.

## 2. Data and methods

### 2.1 Data

There are five kinds of datasets used in this study (Table 1): (1) observed precipitation data; (2) MODIS (Moderate-resolution Imaging Spectroradiometer) LULC category data; (3) DMSP-OLS (the U.S. Air Force Defense Meteorological Satellite Program's Operational Linescan System) nighttime light image; (4) NCEP operational global final (FNL) analysis data; and (5) NCEP RTG_SST (real-time, global, sea surface temperature) data. A more detailed description of these data is provided as follows.

(1) The observed precipitation data used for validation of the simulated Meiyu precipitation and EOF (empirical orthogonal function) analysis in this study are the daily rainfall amounts from 756 stations in China. The measurement method for these precipitation data remained unchanged from 1979 to 2010. The data are of good quality and evenly distributed spatially (Ren et al., 2008).

(2) The MODIS LULC category data (http://duckwater.bu.edu/lc/mod12q1.html) are created using information collected by the Earth Observation System (EOS) for 2001 (hereafter MODIS-2001) and on a 30 arc-seconds resolution grid, covering the global surface. It should be noted that the MODIS-2001 data contain the urban extents in 2001. In this study, the MODIS-2001 data serve as the LULC category data for the WRF model.

(3) The nighttime light images (http://ngdc.noaa.gov/eog/dmsp/downloadV4composites.html) are a group of urban remote sensing products derived from DMSP-OLS with specialized low-light imaging capabilities. The DMSP nighttime light images have provided a continuous time series of urban remote sensing products every year since 1992 and are mapped onto 30 arc-seconds resolution grid, spanning from 65°S to 75°N and 0 to 180°. In this work, the nighttime light images for 2010 are used to derive the urban extents over the YRD in 2010.

(4) The NCEP FNL analysis data (http://rda.ucar.edu/datasets/ds083.2/) are created by the Global Data Assimilation System (GDAS), which continuously collects observational data and other analysis data. The FNL data are on a 1.0°×1.0° resolution grid, and available at the surface and 26 pressure levels from 1000 to 10 hPa every 6 h from July 1999. The FNL data provide the initial and lateral boundary conditions for the large-scale atmospheric fields and initial soil parameters (i.e., soil water, moisture, and temperature) in the WRF simulations.

(5) The NCEP RTG_SST data (http://polar.ncep.noaa.gov/sst/rtg_low_res/), provided by the NCEP/MMAB (Marine Modeling and Analysis Branch), are created using the most recent 24-h buoy and ship data, satellite-retrieved SST data, and satellite-observed sea-ice coverage SST data. The RTG_SST data are on a 0.5°×0.5° resolution grid, and are prepared daily from January 2001. In this research, the RTG_SST data provide the sea surface temperature for the WRF model.

### 2.2 EOF analysis

To investigate the actual precipitation variation

**Table 1.** The datasets used in this study

| Dataset | Time span | Temporal resolution | Spatial coverage | Spatial resolution |
|---|---|---|---|---|
| Observed precipitation | From 1979 | Daily | China | 756 stations |
| MODIS LULC data | 2001 | Annual | Global | 30″×30″ |
| Nighttime light images | From 1992 | Annual | (65°S–75°N, 0°–180°) | 30″×30″ |
| NCEP FNL data | From 1999 | 6 h | Global | 1.0°×1.0° |
| NCEP RTG_SST data | From 2001 | Daily | Global ocean | 0.5°×0.5° |

during the Meiyu period, an EOF analysis for observed precipitation over eastern China was performed. In the current research, a total of 173 out of 756 stations over eastern China (23.5°–38.5°N, 113°–123°E) were used. The observed daily precipitation data were conducted to the pentad anomaly data before the EOF analysis was carried out. In order to compare the Meiyu precipitation variation during 2001–2010 with the year before 2001, and also considering the notable decadal transition of the EASM and corresponding precipitation change over eastern China at the end of the 1970s (Wang, 2001; Yu et al., 2004; Jiang and Wang, 2005; Chen and Xue, 2013), the period for the EOF analysis was selected as 1979 to 2010.

### *2.3 Mapping the MODIS-2010 data*

In order to investigate the impacts of urban expansion on precipitation during the Meiyu season, MODIS LULC category data providing a realistic impression of urban expansion are required. The MODIS-2001 data, which contain the urban extents in 2001, serve as the underlying surface LULC category data in the WRF model. However, MODIS LULC data that include the urban extents for 2010 are absent. Therefore, we had to derive the urban distribution for 2010 from another data source. Nighttime light images have been widely used as a proxy for variables that are difficult to measure directly (Elvidge et al., 2013), such as population (Doll, 2008), economic activity (Ghosh et al., 2010), and urban extent (Small et al., 2005; He et al., 2006; Yang et al., 2011). Generally speaking, regions with large nighttime light values are most likely representative of an urban area. He et al. (2006) developed a technique for efficiently and quickly deriving urban land information from DMSP-OLS nighttime light images. One of the most important foundations of the approach is that the area of urban extents (i.e., the regions where the nighttime light value is larger than the urban nighttime light threshold) derived from the nighttime light image should be closer or equal to the "true" urban area from statistical data, such as the *China Land and Resources Statistical Yearbook (He et al., 2006).* Therefore, this method can largely reflect the quantitative characteristics of urban areas. Table 2 shows the urban nighttime light thresholds for deriving the urban extents in 2010 over Shanghai, Jiangsu, and Zhejiang.

**Table 2.** Urban nighttime light thresholds for deriving urban extents in 2010

| | Shanghai | Jiangsu | Zhejiang |
|---|---|---|---|
| MODIS-2010 | 57 | 54 | 54 |

The urban land information was firstly removed over the YRD within the MODIS-2001 LULC data, and then the urban distribution for 2010 derived from the nighttime light image was mapped to the same region of MODIS-2001, ultimately deriving the MODIS LULC category for 2010 (hereafter MODIS-2010). Figure 1 shows the distribution of the MODIS-2001 and MODIS-2010 LULC categories over the YRD. Table 3 indicates that the urban area in the YRD in 2001 was 9537 km$^2$ and accounted for 15.9% of the total land area, while the urban area was 14051 km$^2$ and accounted for 23.4% of the total land area in 2010. The urban expansion over the YRD during 2001–2010 is clear.

## 3. Model and numerical experiments

### *3.1 Model configuration*

The regional meteorological model used in this study is the WRF version 3.3.1 with the Advanced Research WRF (ARW) dynamics solver (Skamarock et al., 2008). WRF is a fully compressible and Euler nonhydrostatic model with multiple options for physical parameterization, which can be applied for simulations across scales ranging from large-eddy to global (Zhang et al., 2011). Table 4 shows the parameterization schemes selected for the model physical processes in the simulation. A more detailed presentation of this information is provided as follows.

The WRF single-moment six-class (WSM6) microphysics scheme (Hong and Lim, 2006) and new Kain-Fritsch convective parameterization scheme (Kain, 2004) were selected for simulating the precipitation process in current study. The WSM6 scheme contains six prognostic water substance variables, i.e., the mixing ratios of water vapor, rain, snow, graupel, cloud ice, and cloud water. The new Kain-Fritsch scheme utilizes a cloud model which contains the ef-

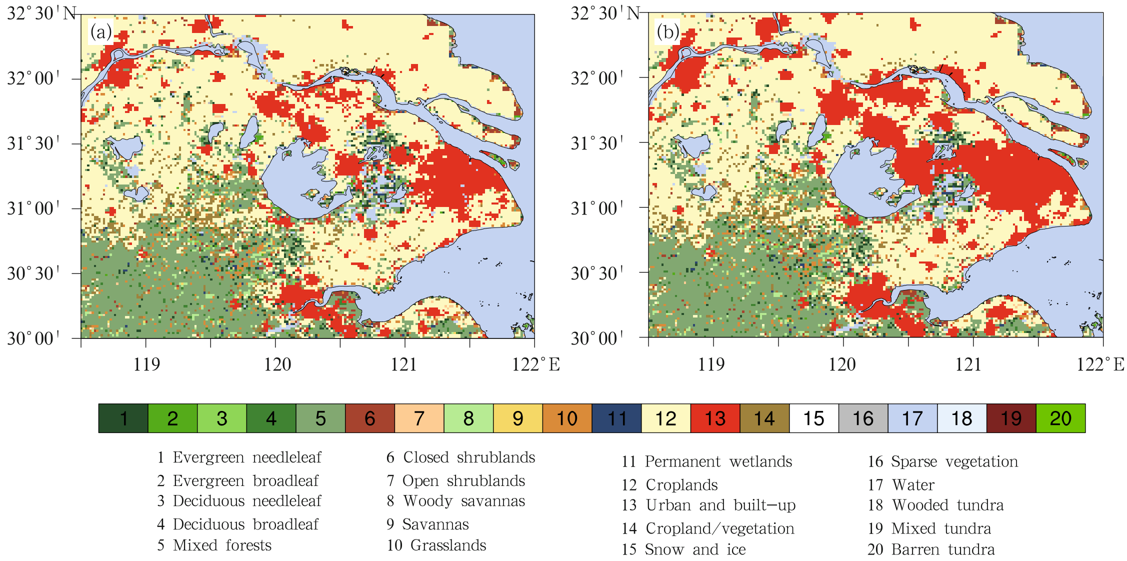


**Fig. 1.** Distribution of MODIS LULC categories in (a) 2001 and (b) 2010 for the YRD.

**Table 3.** 2001 and 2010 urban areas and urbanized ratios (urban area divided by total land area) in the YRD

| Year | Urban area (km$^2$) | Urbanized ratio (%) |
|---|---|---|
| 2001 | 9537 | 15.9 |
| 2010 | 14051 | 23.4 |

fects of detrainment, entrainment, and relatively simple microphysics.

The unified Noah land surface model (LSM) (Chen and Dudhia, 2001) was selected for the land surface process. The Noah LSM consists of one canopy layer and four soil layers with depths of 10, 30, 60, and 100 cm. It can predict skin temperature and moisture, which is important in regional climate simulation, as moisture feedback plays an important role in air-land surface interaction (Bukovsky and Karoly, 2009).

The Yonsei University (YSU) planetary boundary layer (PBL) scheme (Hong et al., 2006) was used to represent the boundary layer and sub-grid scale processes. The YSU scheme uses countergradient terms to represent fluxes due to both local and nonlocal gradients. It consists of an enhanced stable boundary layer diffusion algorithm that allows deeper mixing in windier conditions.

In addition, the atmospheric long- and shortwave radiation was calculated every 30 minutes using the NCAR Community Atmosphere Model (CAM 3.0) spectral band longwave and shortwave radiation scheme (Collins et al., 2006).

### *3.2 Numerical experiment design*

Two groups of long-term simulations using MODIS-2001 and MODIS-2010 LULC category data were performed (hereafter referred to as experiment M01 and M10, respectively). Each group covered 10 summers from 2001 to 2010, and each summer was initialized on 26 May. The first 6 days (26–31 May) of each simulation were used as the model spin-up period to minimize the initialization effects of soil moisture and soil temperature. As shown in Table 5, both

**Table 4.** Choices of the primary physical parameterization schemes of WRF

| Physical process | Parameterization scheme |
|---|---|
| Microphysics | WSM 6-class scheme (Hong and Lim, 2006) |
| Cumulus parameterization | New Kain-Fritsch convective scheme (Kain, 2004) |
| Land surface process | Noah land surface model (Chen and Dudhia, 2001) |
| Planetary boundary layer process | YSU scheme (Hong et al., 2006) |
| Longwave and shortwave radiation | CAM3 longwave and shortwave radiation scheme (Collins et al., 2006) |

groups used the 30-km horizontal grid resolution and 28 terrain-following vertical layers. The model domain consisted of 161 (west–east)×161 (south–north) grid points and was centered at 30.5°N, 115°E, covering East Asia and its adjacent oceans. The FNL data provided initial and lateral boundary conditions for the simulation and RTG_SST data served as the sea surface temperature because updating SST is important for improving precipitation simulations as a result of more realistic depiction of wind and moisture flux (Bukovsky and Karoly, 2009).

**Table 5.** Setup of the numerical experiments

| Group | M01 | M10 |
|---|---|---|
| Grid resolution | 30 km | 30 km |
| Horizontal grids | 161×161 | 161×161 |
| Vertical layers | 28 | 28 |
| Initial date | May 26 | May 26 |
| Years | 2001–2010 | 2001–2010 |
| Initial and lateral conditions | FNL | FNL |
| SST | RTG_SST | RTG_SST |
| LULC category data | MODIS-2001 | MODIS-2010 |

## 4. Results

### *4.1 Validation of the WRF model*

The capability of the WRF model in simulating the climate over eastern China in the Meiyu season is first evaluated by comparing the precipitation, air temperature, and pseudo-equivalent temperature produced by experiment M10 with the observed and analysis data. The observed precipitation and 2-m air temperature are obtained from 756 meteorological stations in China, and the isobaric surface temperature and pseudo-equivalent temperature are provided by the NCEP FNL data. In the current study, the Meiyu season is from the third pentad in June to the fourth pentad in July.

Figure 2 presents the observed and WRF-simulated 10-yr climatic precipitation during the Meiyu period. As shown in Fig. 2a, the observed precipitation exhibits a spatial distribution pattern with more precipitation in the southeast of eastern China (> 8 mm day$^{-1}$) and less precipitation over regions to the north of 36°N (< 3.5 mm day$^{-1}$). We find that the WRF model captures well both the magnitude and geographical distribution of observed precipitation over most parts of eastern China (Fig. 2b). A major difference between the WRF-simulated and observed precipitation (Fig. 2c) is that the WRF model tends to simulate more (less) rainfall than is actually the case

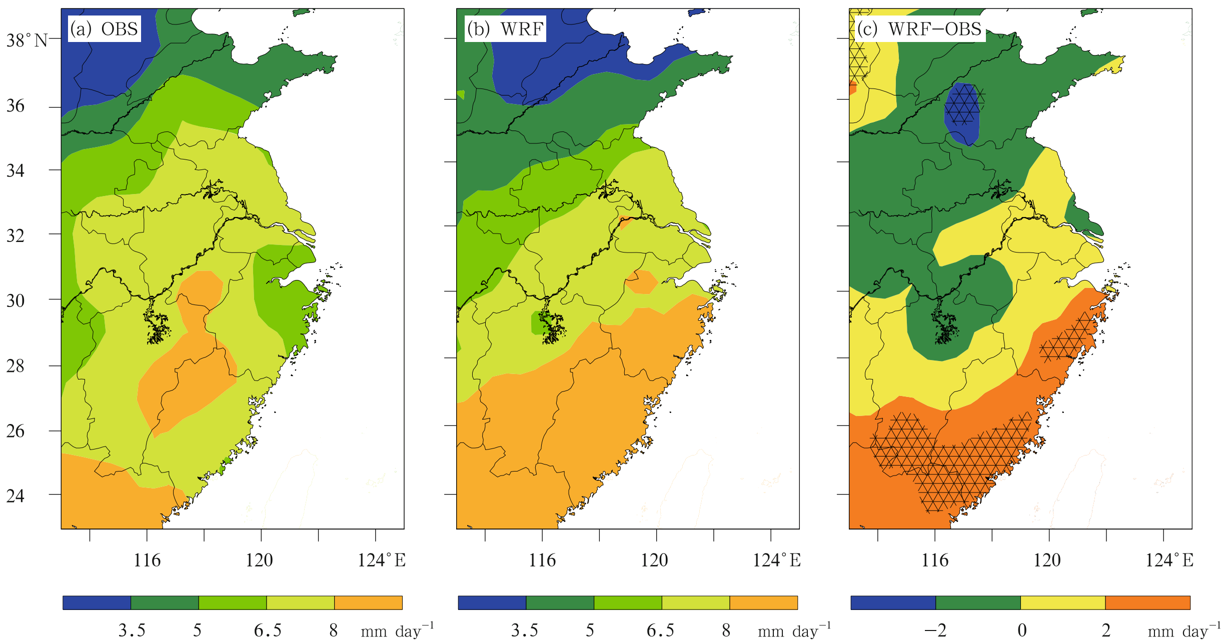


**Fig. 2.** (a) Observed and (b) WRF-simulated climatological precipitation during the 2001–2010 Meiyu seasons, and (c) the difference between the two. Black grids denote regions where the difference is statistically significant at the 99% confidence level.

over the southeast (northwest) parts of eastern China. In addition, we also find that this difference between the WRF-simulated and observed precipitation is not significant over most parts of eastern China, except over western Shandong and regions to the south of Jiangxi, Fujian, and Zhejiang provinces.

Figure 3 presents the standard deviation of observed and WRF-simulated precipitation during the 2001–2010 Meiyu seasons. We can see that the spatial pattern of the standard deviation of observed precipitation (Fig. 3a) is similar to the pattern of climatic precipitation (Fig. 2a). A major difference in the pattern between the standard deviation and climatic precipitation is that there are two large-value centers located over the Yangtze-Huaihe River basin and regions between Jiangxi and Fujian. As shown in Fig. 3b, the WRF model is able to reproduce the dominant features of the standard deviation of precipitation during the Meiyu period. However, the standard deviation of the simulated precipitation is smaller than that of the observation over southern Shandong, northern Jiangsu, and southern Jiangxi, but larger over other regions of eastern China (Fig. 3c). It is also noted that the difference in the standard deviation between the WRF-simulated and observed precipitation is not significant over eastern China.

Figure 4a shows the time series of the observed and WRF-simulated 10-yr (2001–2010) climatological pentad precipitation regionally averaged over the Yangtze-Huaihe River basin (28°–35°N, 110°–120°E; Huang et al., 2011). We can see that the observed precipitation increases from June to July and there are two precipitation peaks in the second (8.4 mm day$^{-1}$) and fifth (7.4 mm day$^{-1}$) pentads in July, after which the precipitation decreases. It is clear that the WRF model is able to simulate well the dominant features of the temporal variation of precipitation in the Meiyu season. The correlation coefficient between the observed and simulated precipitation is 0.85, which is statistically significant at the 99% confidence level.

Figure 4b shows the time series of the observed and WRF-simulated 10-yr climatological pentad 2-m air temperature regionally averaged over the Yangtze-Huaihe River basin. We can see that the observed 2-m air temperature increases rapidly from the first pentad in June to the first pentad in July, after which it increases slowly to the sixth pentad in July. We can also see that the 2-m temperature possesses a decreas-

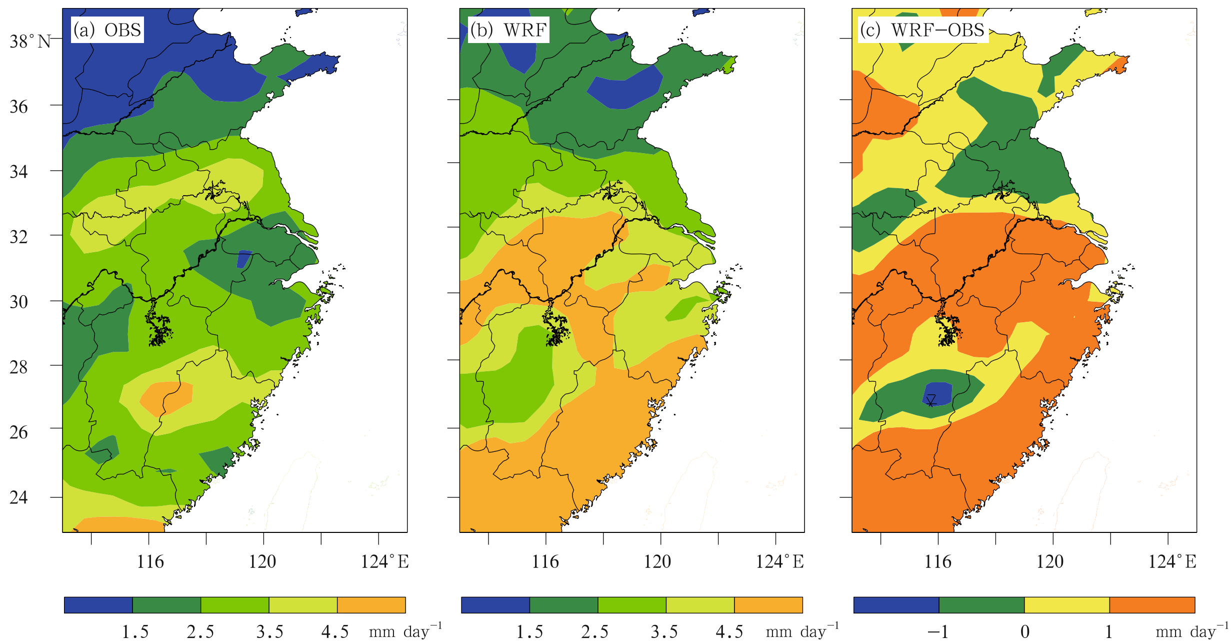


**Fig. 3.** Distributions of standard deviation of (a) observed and (b) WRF-simulated precipitation during the 2001–2010 Meiyu seasons, and (c) the difference between the two.

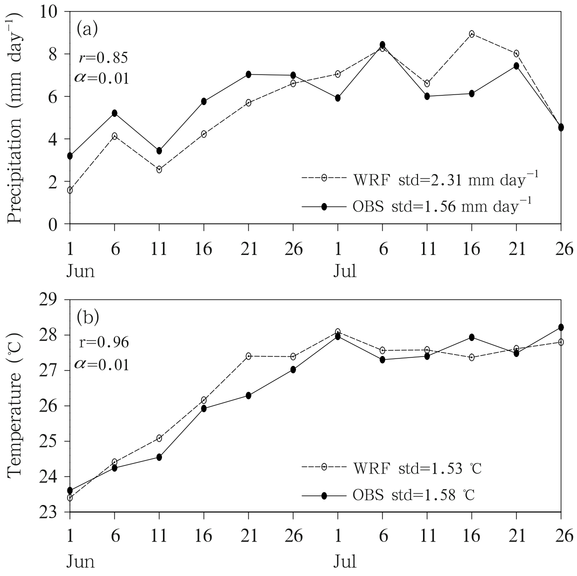


**Fig. 4.** Time series of (a) observed and WRF-simulated 10-yr (2001–2010) climatological pentad precipitation and (b) 2-m air temperature regionally averaged over the Yangtze-Huaihe River basin (28°–35°N, 110°–120°E) (std: standard deviation; $r$: correlation coefficient; $\alpha$: correlation coefficient at the 99% confidence level).

ing trend in the second and fifth pentads in July, as a result of more precipitation in these two pentads. The WRF model reproduces well the characteristics of the temporal variation of the 2-m air temperature in the Meiyu season. The correlation coefficient between the observed and simulated 2-m temperature is 0.96, which is statistically significant at the 99% confidence level.

Since the gradient of the pseudo-equivalent temperature can indicate the position of the Meiyu front and heavy precipitation belt, it is important to evaluate the capability of the WRF model in simulating the distribution and magnitude of the pseudo-equivalent temperature. Figure 5 shows the height-latitude cross-section of the FNL analysis and WRF-simulated air temperature and pseudo-equivalent temperature averaged along 105°–125°E. As shown in Fig. 5a, the large pseudo-equivalent temperature gradient belt extends from the surface to 700 hPa over the regions between 28° and 36°N and a warm air column is located to the south of the large pseudo-equivalent temperature gradient belt. It is clearly shown in Fig. 5b that the WRF model simulates well the air temperature and pseudo-equivalent temperature distribution with close magnitudes. Moreover, the WRF model can reproduce the large pseudo-equivalent temperature gradient belt and the warm air column.

Overall, the WRF model exhibits good ability in reproducing the major features of the climate over eastern China during the Meiyu period. This gives

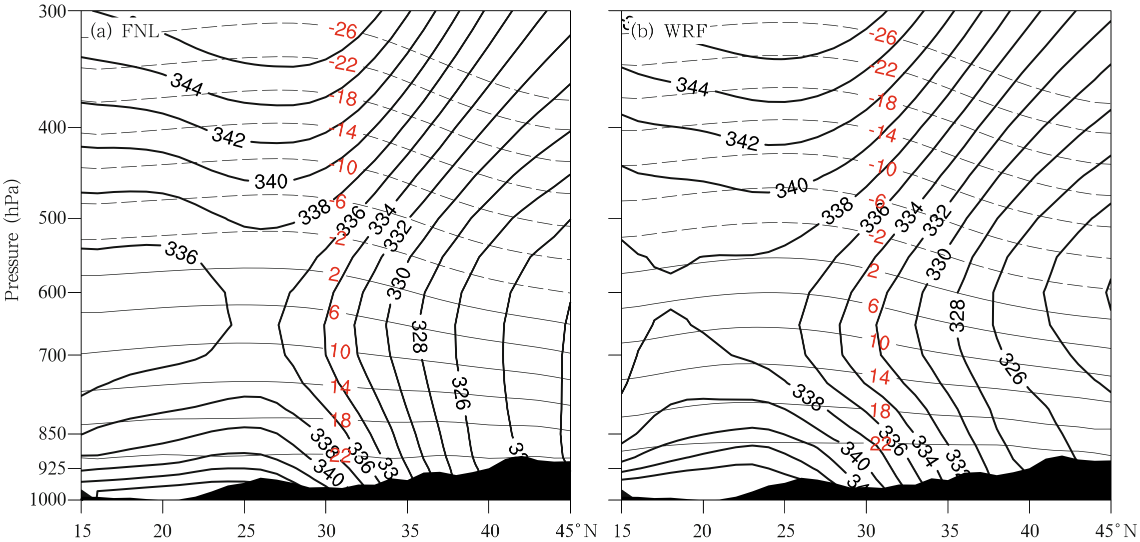


**Fig. 5.** Height-latitude cross-sections of the 10-yr (2001–2010) climatological air temperature (℃; thin line) and pseudo-equivalent temperature (K; thick line) averaged along 105°–125°E in the Meiyu season from (a) FNL analysis data and (b) WRF-simulated data. The black shading indicates the terrain.

us confidence to use the model's output to study the impacts of urban expansion on the precipitation in the Meiyu season.

### *4.2 Impacts of urban expansion on Meiyu precipitation*

A previous study indicated that the enhanced convergence due to increased surface roughness and destabilization due to the urban heat island (UHI) perturbation of the planetary boundary layer in urban areas lead to regional precipitation change (Wang et al., 2012). It is therefore reasonable to hypothesize that urban expansion modifies the roughness and thermal conductivity of the original land surface, and may also cause regional precipitation change. Figure 6 shows the changes in total, cumulus, and grid-scale precipitation (difference between M10 and M01) during the Meiyu period induced by urban expansion in the YRD averaged over 2001–2010. It is clear that the urban expansion results in a decrease (increase) of total precipitation over the regions to the north of 35°N and the Yangtze River basin (Huaihe River basin and the south of 28°N) with an intensity of 0.2–1.2 mm day$^{-1}$ (Fig. 6a). As shown in Fig. 6b, the pattern of cumulus precipitation change induced by urban expansion is similar to that of total precipitation change over most parts of eastern China except the YRD and western Shandong, which indicates that the change of cumulus precipitation contributes to the total precipitation change. In addition, it is found that the grid-scale precipitation change also contributes to the total precipitation change (Fig. 6c).

To investigate the relationship between the impacts of urban expansion and the actual precipitation change during the Meiyu period, an EOF analysis for observed precipitation over eastern China was performed. Figure 7 shows the first three leading EOF modes and the corresponding time series of the principal components (PCs) of the observed pentad precipitation over eastern China during the 1979–2010 Meiyu seasons. The first three leading EOF modes explain 19.06%, 17.79%, and 8.17% of the total variance, respectively. Figure 7a shows that the spatial distribution of EOF-1 is characterized by a "+, –" pattern,

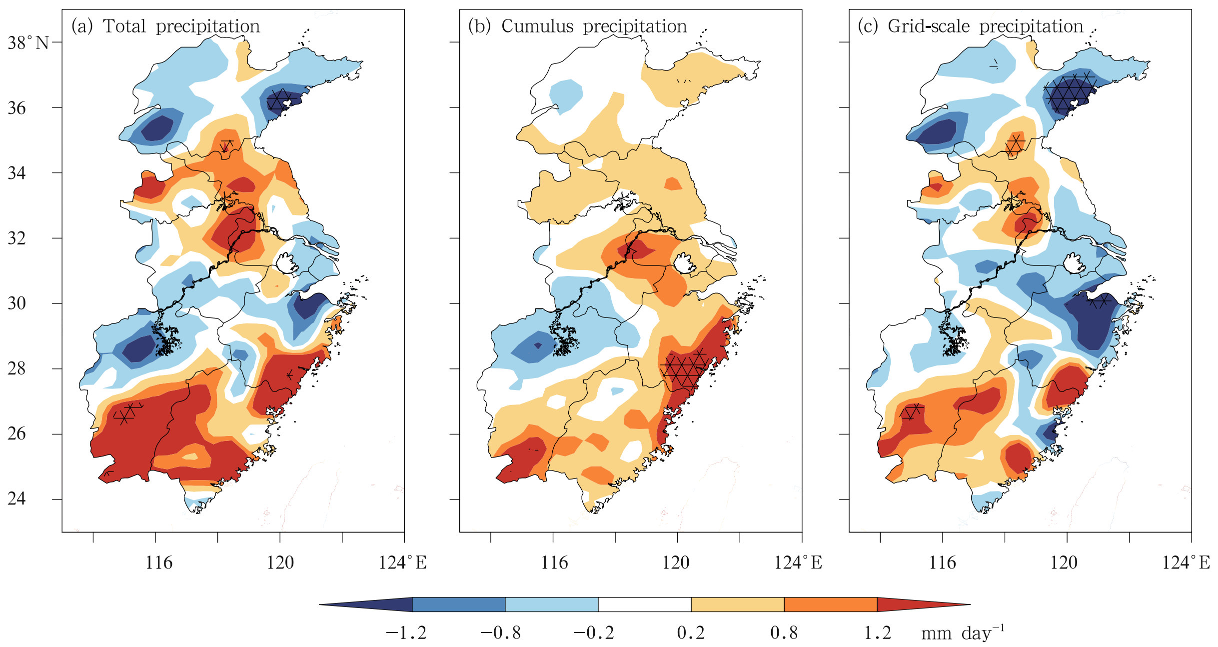


**Fig. 6.** Changes in (a) total, (b) cumulus, and (c) grid-scale precipitation (difference between M10 and M01) induced by urban expansion in the YRD and averaged during the 2001–2010 Meiyu periods. Black grids denote those regions where the change of precipitation is statistically significant at the 90% confidence level.

with the latitude of 30°N as the division. Meanwhile, PC-1 (Fig. 7d) indicates that the Meiyu precipitation increases (decreases) over the regions to the north of 30°N but decreases (increases) over the regions to the south of 30°N from the end of the 1970s to the early 1990s and from the early 1990s to the early 2000s. The spatial distribution of EOF-2 (Fig. 7b) is characterized by a "–, +, –" pattern over eastern China, and PC-2 (Fig. 7e) implies that the Meiyu precipitation over the regions between 26° and 34°N (regions to the north of 34°N and to the south of 26°N) increases (decreases) from the end of the 1970s to the end of the 1990s but decreases (increases) in the 2000s. Different from the first two leading modes, the EOF-3 (Fig. 7c) and PC-3 (Fig. 7f) indicate that the Meiyu precipitation increases (decreases) over the Huaihe River basin (30°–34°N ) and the south of 27°N (Yangtze River basin (27°–30°N) and north of 34°N) since the mid 1990s. It can be seen that the Meiyu belt has a decadal northward-moving trend after the early 2000s. Previous studies have suggested that the possible mechanisms underlying the Meiyu belt northward movement are: (1) a tropospheric warming and stratospheric cooling trend in the midlatitudes of East Asia (Si et al., 2009), and (2) the interdecadal change of land-sea thermal contrast in East Asia (Liu et al., 2012).

In addition, it is noted that both the spatial distribution and magnitude of EOF-3 (Fig. 7c) are consistent with the total precipitation change (Fig. 6a). To further investigate the relationship between the EOF-3 and simulated precipitation change induced by urban expansion, the simulated pentad total, cumulus, and grid-scale precipitation changes (M10 minus M01)

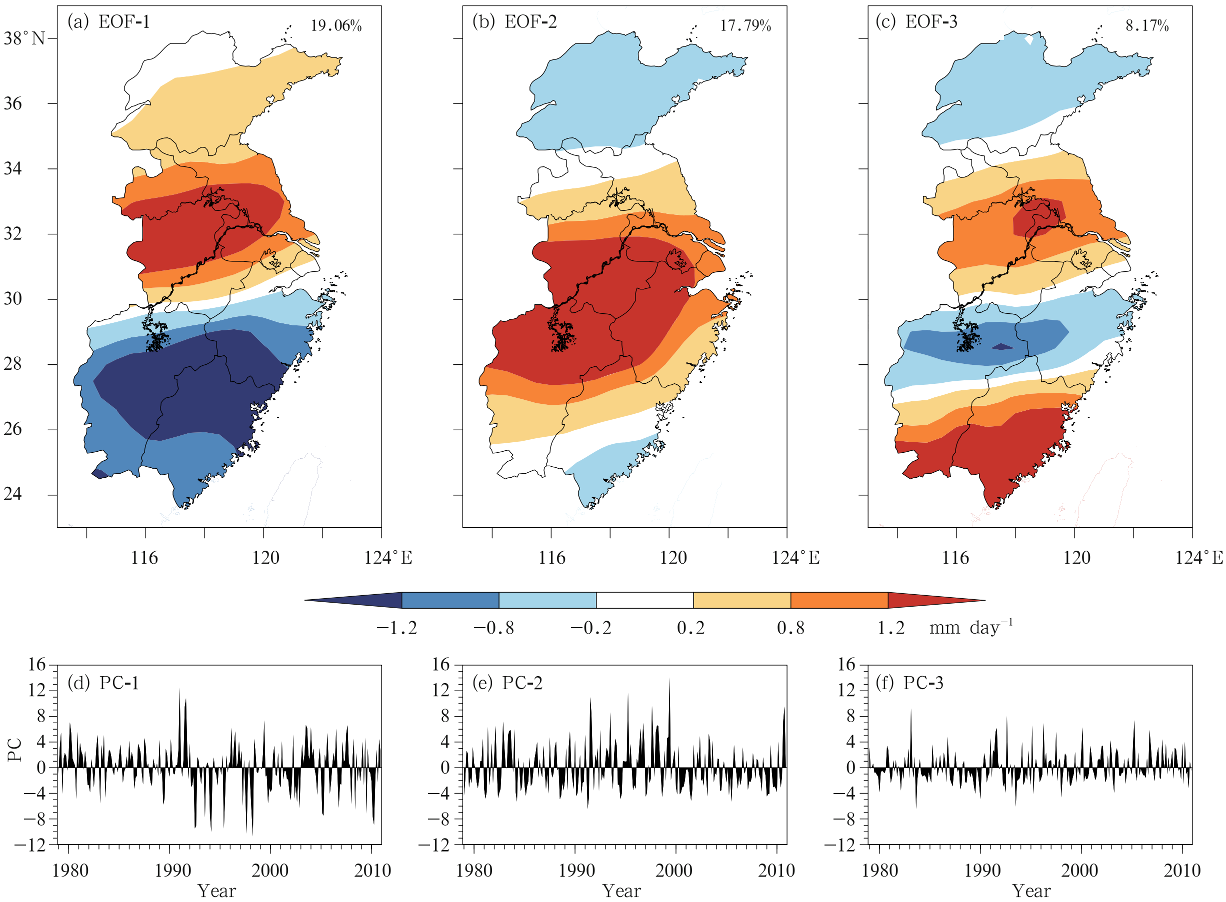


**Fig. 7.** (a, b, c) The first three leading EOF modes and (d, e, f) corresponding time series of the anomaly principal components (PCs) of the observed pentad precipitation at 173 stations over eastern China during the 1979–2010 Meiyu seasons.

during the 2001–2010 Meiyu seasons are projected onto the spatial pattern of the EOF-3, deriving three groups of time series (Figs. 8a–c). We can see that the time series of the projection of the simulated pentad total, cumulus, and grid-scale precipitation changes are consistent with the PC-3 since 2005, because the actual urban expansion over the YRD revealed by MODIS-2001 and MODIS-2010 occurs after 2005. Moreover, the simulated pentad total, cumulus, and grid-scale precipitation changes during the 2001–2010 Meiyu seasons are projected onto the spatial patterns of the first six leading EOF modes, and the correlation coefficients between the time series of the projection and observed PCs during 2005–2010 are calculated for each mode (Figs. 8d–f). We find that the correlation coefficient between the projection series of total precipitation change and the PC-3 is positive and the magnitude (0.33; statistically significant at the 95% confidence level) is the largest (Fig. 8d). Similar results are found for the cumulus and grid-scale precipitation changes (Figs. 8e and 8f). Overall, it can be concluded that the spatiotemporal pattern of the EOF-3 mode of observed precipitation is related to the urban expansion in the YRD.

### *4.3 Impacts of urban expansion on humidity, evaporation, and circulation*

To investigate the reason for the Meiyu precipitation change, the impacts of urban expansion on air humidity, surface evaporation, and atmospheric circulation are examined. Figure 9a shows that the 10-yr (2001–2010) climatological tropospheric (950–400

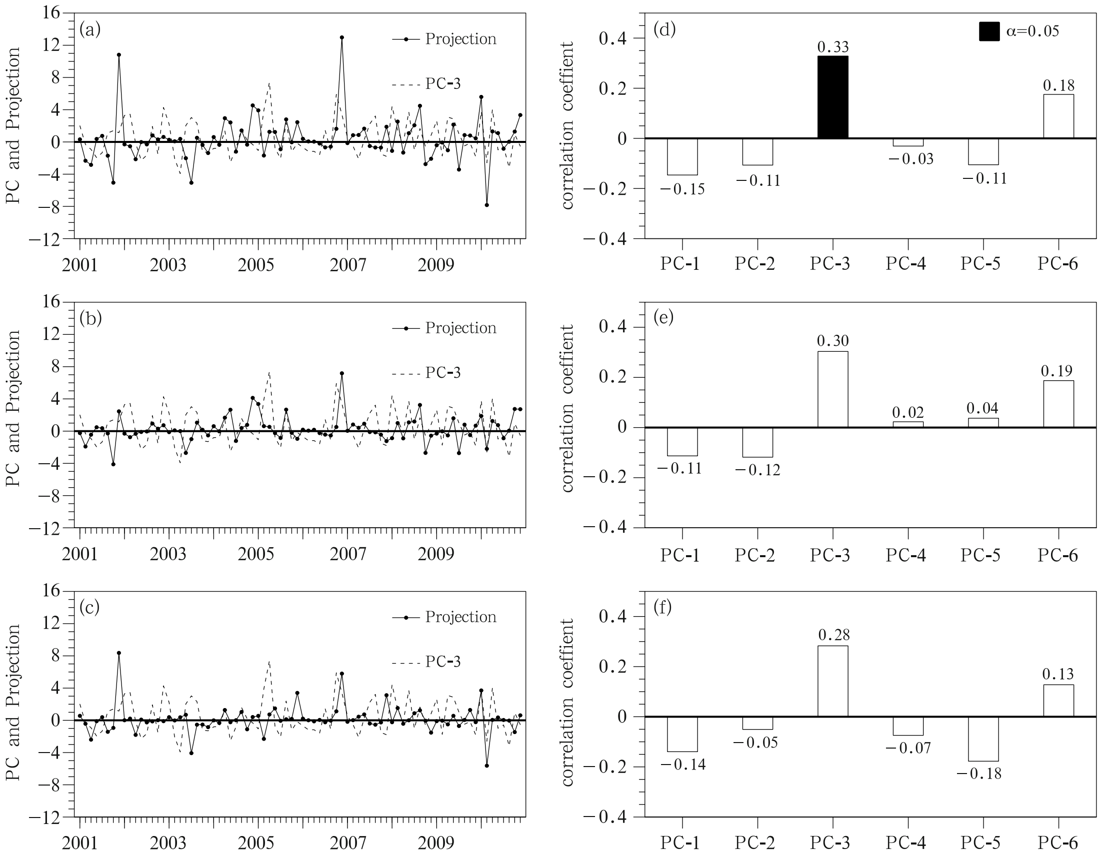


**Fig. 8.** Time series of the observed PC-3 and projection of the pentad-simulated (a) total, (b) cumulus, and (c) grid-scale precipitation changes (M10 minus M01) onto the EOF-3. The correlation coefficients calculated between the projection time series of the pentad-simulated (d) total, (e) cumulus, and (f) grid-scale precipitation changes onto the EOFs and observed PCs during 2005–2010 for the first six leading EOF modes are also presented. The black column in (d) denotes correlation statistically significant at the 95% confidence level.

hPa) air humidity increases from north to south over eastern China. This pattern leads to more precipitation in the southeast of eastern China and less precipitation over regions to the north of 36°N (Fig. 2). Further analysis indicates that the spatial pattern of the tropospheric air humidity change induced by urban expansion (Fig. 9b) with the intensity increased (decreased) over the regions of 31°–36°N and to the south of 27°N (north of 36°N and (27°–31°N, 114°–119°E)), corresponds well to that of cumulus (Fig. 6b) and grid-scale (Fig. 6c) precipitation changes during the Meiyu period over most parts of eastern China. Therefore, the implication, is that the changed tropospheric air humidity is a major reason for the Meiyu precipitation change, which is induced by urban expansion. However, we also find that the tropospheric air humidity increases over the YRD while the grid-scale precipitation decreases over the same region, which indicates that the grid-scale precipitation over the YRD is affected by other factors.

Urban expansion can change the level of evaporation by modifying surface physical properties. Figure 10 shows the 10-yr climatological surface evaporation and its change induced by urban expansion. As shown in Fig. 10a, surface evaporation also increases from north to south over eastern China and a high-value center is located at 27°N over land. We find that urban expansion over the YRD results in an increase (decrease) of surface evaporation over the regions between 32° and 36°N, as well as in Zhejiang and Fujian provinces (regions between 30° and 32°N, as well as Jiangxi and Shandong provinces) over eastern China (Fig. 10b). Moreover, it is noted that surface evaporation over the YRD is significantly reduced at the 90% confidence level, which leads to decreased grid-scale precipitation during the Meiyu period over the YRD (Fig. 6c), ultimately causing the decreasing trend of total precipitation (Fig. 6a).

Because vertical motion is one of the most important factors affecting precipitation, the impact of

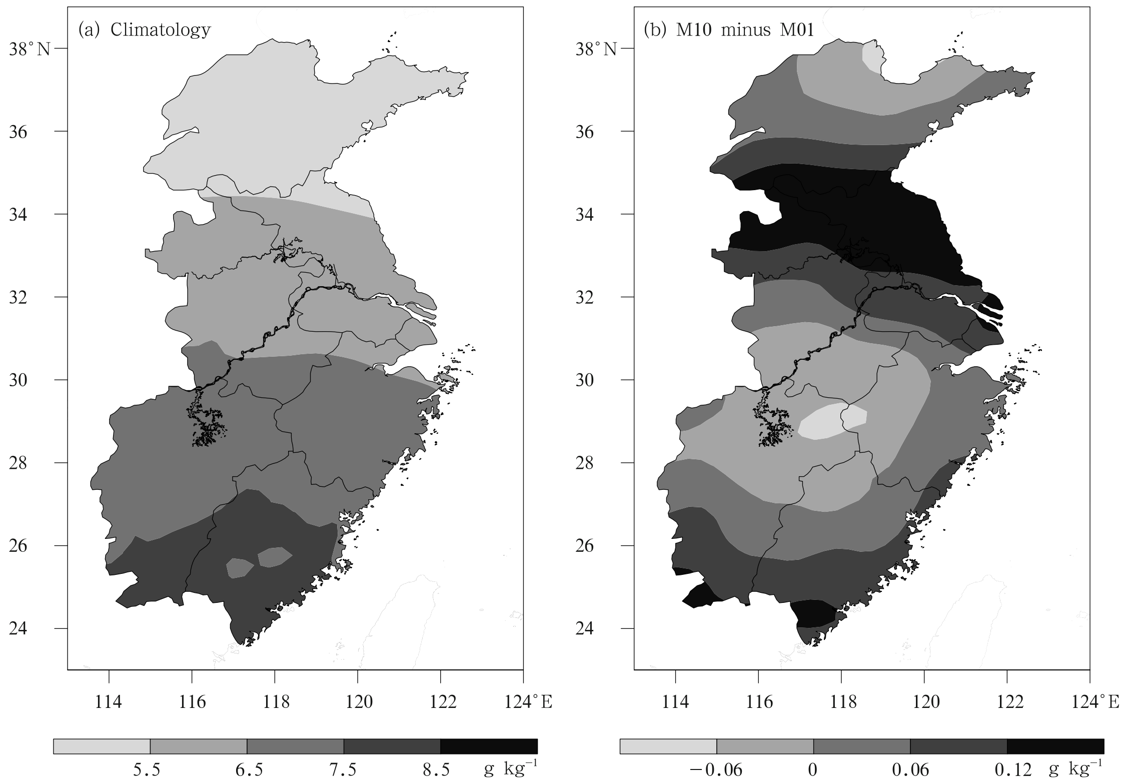


**Fig. 9.** Distributions of the 10-yr (2001–2010) (a) climatological (M01) tropospheric (950–400 hPa) specific humidity and (b) change of tropospheric specific humidity induced by urban expansion (M10 minus M01) over eastern China during the Meiyu season.

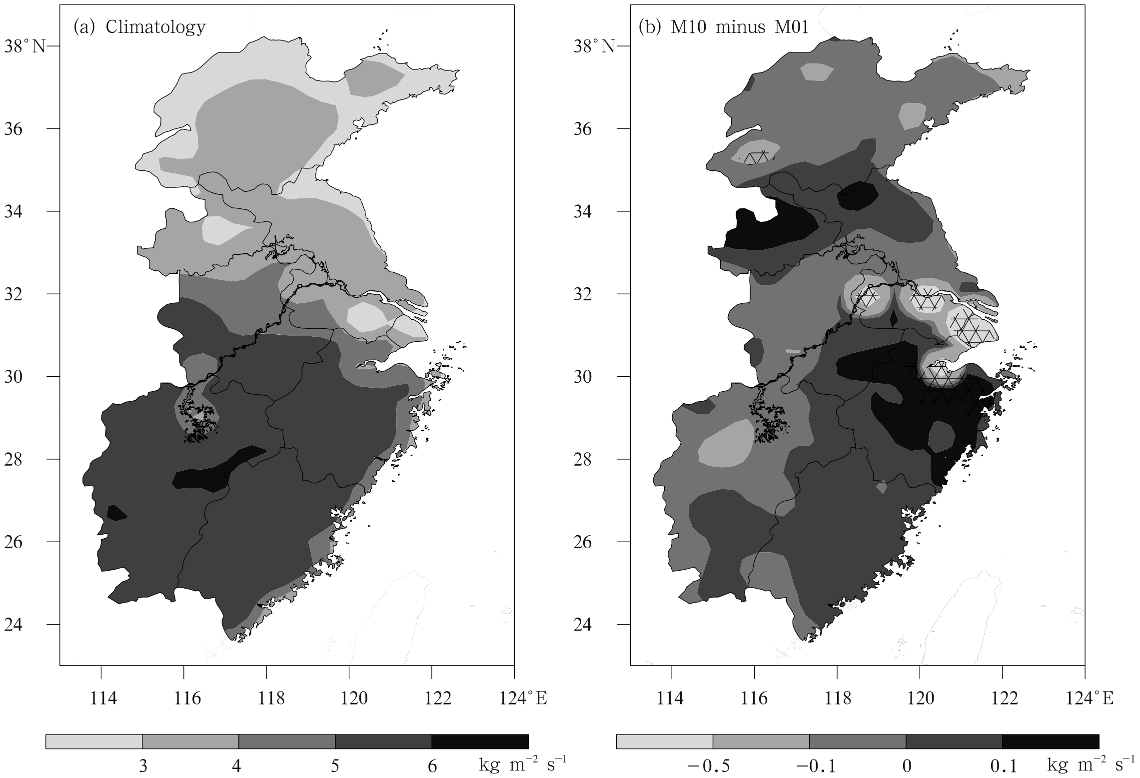


**Fig. 10.** As in Fig. 9, but for surface evaporation. Black grids denote those regions where the change is statistically significant at the 90% confidence level.

urban expansion on atmospheric vertical velocity is also analyzed. Figure 11 shows the spatial distribution of climatological tropospheric vertical velocity and the change of tropospheric vertical velocity induced by urban expansion. We find that the climatological upward motion (Fig. 11a; negative values) over the regions to the south of 35°N causes more precipitation during the Meiyu period (Fig. 2). As shown in Fig. 11b, the change in tropospheric vertical velocity induced by urban expansion reveals a pattern with an increased (decreased) trend over the Yangtze River basin and the region north of 35°N (Huaihe River basin and the region south of 28°N), indicating that anomalous downward (upward) motion occurs over corresponding regions and leads to decreased (increased) simulated precipitation change over the Yangtze River basin and the region north of 35°N (Huaihe River basin and the region south of 28°N).

To study the reason for the changes in tropospheric air humidity and vertical motion, the impacts of urban expansion on atmospheric circulation and moisture transport should also be analyzed. Figure 12 shows distributions of climatological moisture transport and its divergence, and their changes induced by urban expansion. As shown in Fig. 12a, southwest (northwest) wind and moisture transport can be found over eastern China and its adjacent sea to the south (north) of 32°N. The implication is that the convergence (divergence) of circulation and moisture transport located between 28° and 33°N (regions to the north of 34°N) lead to more (less) air humidity (Fig. 9a) and upward (downward) vertical motion (Fig. 11a) over the corresponding regions. Moreover, the urban expansion over the YRD causes the horizontal circulation and moisture transport to change, as shown in Fig. 12b. It is noted that an anomalous anticyclone locates over the East China Sea, while an anomalous cyclone locates to the east of Taiwan. This anomalous circulation pattern leads to the convergence (divergence) of horizontal circulation and moisture trans-

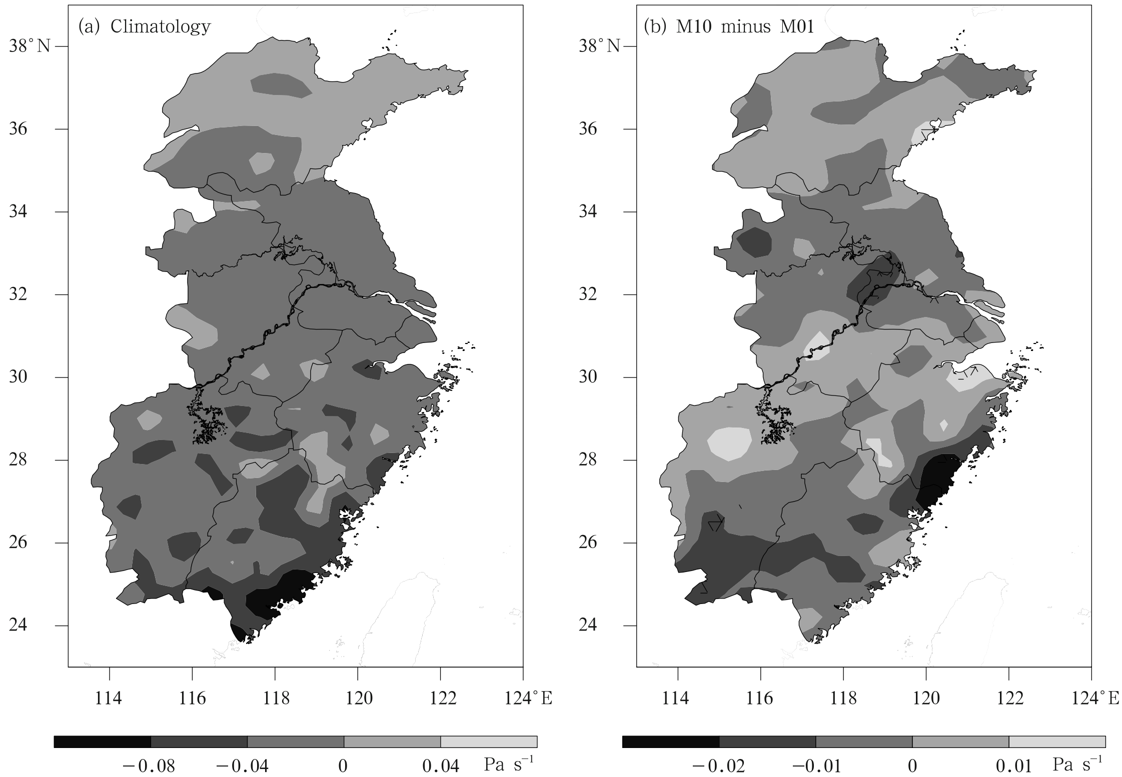


**Fig. 11.** As in Fig. 9, but for tropospheric (950–400 hPa) vertical velocity. Negative values denote upward motion and positive values downward motion.

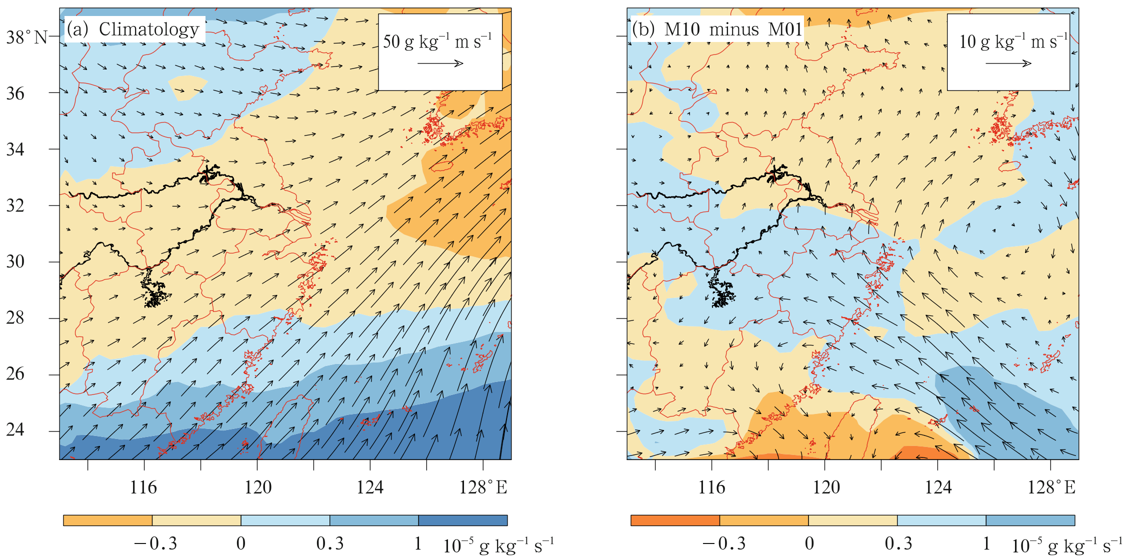


**Fig. 12.** As in Fig. 9, but for tropospheric (950–400 hPa) moisture transport (vectors) and divergence of moisture (shading). Negative values denote convergence of moisture and positive values divergence of moisture.

port over the regions to the north of 32°N and to the south of 28°N (regions between 28° and 32°N), ultimately causing the changes of vertical motion (Fig. 11b) and air humidity (Fig. 9b).

### *4.4 Impacts of urban expansion on surface energy balance and temperature*

To further investigate the reason for the change of atmospheric circulation, the changes of surface energy balance and temperature are studied. As described by Su (2002), the surface energy balance can be written as

$$R_{\mathrm{n}} = G_0 + H + \lambda E, \tag{1}$$

where $R_{\mathrm{n}}$ and $G_0$ are surface net radiation and soil heat flux, respectively, defined as positive in the downwards direction; $H$ and $\lambda E$ are the surface sensible and latent heat fluxes, respectively; $\lambda$ is the latent heat of vaporization and $E$ is the actual evapotranspiration. $H$ and $\lambda E$ are defined as positive in the upwards direction. The equation to calculate the surface net radiation is

$$R_{\mathrm{n}} = (1-\alpha)R_{\mathrm{swd}} + \varepsilon R_{\mathrm{lwd}} - \varepsilon\sigma T_{\mathrm{skin}}^4, \tag{2}$$

where $\alpha$ is the surface albedo, $R_{\mathrm{swd}}$ is the downward solar radiation, $R_{\mathrm{lwd}}$ is the downward longwave radiation, $\varepsilon$ is the emissivity of the surface, $\sigma$ is the Stenfan-Bolzmann constant, and $T_{\mathrm{skin}}$ is the surface skin temperature. $R_{\mathrm{swd}}$ and $R_{\mathrm{lwd}}$ are both defined as positive in the downwards direction. It can be derived from Eqs. (1) and (2) by

$$E_{\mathrm{in}} = (1-\alpha)R_{\mathrm{swd}} + \varepsilon R_{\mathrm{lwd}} - G_0 - H - \lambda E, \tag{3}$$

$$R_{\mathrm{up}} = \varepsilon\sigma T_{\mathrm{skin}}^4, \tag{4}$$

$$E_{\mathrm{in}} = R_{\mathrm{up}}, \tag{5}$$

where $E_{\mathrm{in}}$ denotes the surface net incoming energy and $R_{\mathrm{up}}$ denotes the surface upward longwave radiation. In long-term simulations, the surface net incoming energy $E_{\mathrm{in}}$ should equal the surface upward longwave radiation $R_{\mathrm{up}}$.

As shown in Fig. 13a, the urban expansion over the YRD results in increased surface incoming energy over most parts of eastern China, especially in the YRD and western Shandong where the increased surface incoming energy has an intensity of greater than 2 W m$^{-2}$. As a result of the increased surface incoming net energy, the skin temperature also increases over most parts of eastern China, and the increase in intensity is greater than 0.4 in the YRD and western Shandong (Fig. 13c). Because the surface upward longwave radiation is positively correlated with skin temperature (Eq. (4)), the spatial pattern of the changed surface upward longwave radiation (Fig. 13b) induced by urban expansion is closer to that of skin temperature, and this leads to the surface energy reaching a new balanced status. Affected by the skin temperature, the 2-m air temperature also increases over most parts of eastern China (Fig. 13d). Therefore, the implication is that the urban expansion in the YRD strengthens the land-sea thermal contrast over eastern China and the adjacent sea, which further causes changes in atmospheric circulation and moisture transport.

Further analysis indicates that the urban expansion in the YRD can result in increased air temperature from the surface to 250 hPa over the north of 30°N, and the warm air column can even extend upward to the 150-hPa level over the south of 27°N (Fig. 14). It is also noted that there are three high-value centers of increased air temperature. One center is located between 30° and 35°N, extending upward from 650 to 300 hPa with an intensity above 0.16, while the other two are located between 30° and 33°N and to the north of 36°N, extending from the surface to 850 and 700 hPa with an intensity above 0.24 and 0.2, respectively. However, the urban expansion in the YRD leads to decreased air temperature above 200 hPa (150 hPa) over the north of 34°N (the south of 27°N), and the cool air column can extend downward to 300 hPa between 28° and 30°N. The implication is that urban expansion in the YRD could be a cause of the tropospheric warming and stratospheric cooling trend over eastern China.

## 5. Conclusions

The precipitation during the Meiyu period has experienced an increasing trend in the Huaihe River basin and a decreasing trend in the Yangtze River basin in recent years, while at the same time, the YRD has experienced remarkably rapid urban expansion. In this study, two WRF simulation scenarios (M01 and

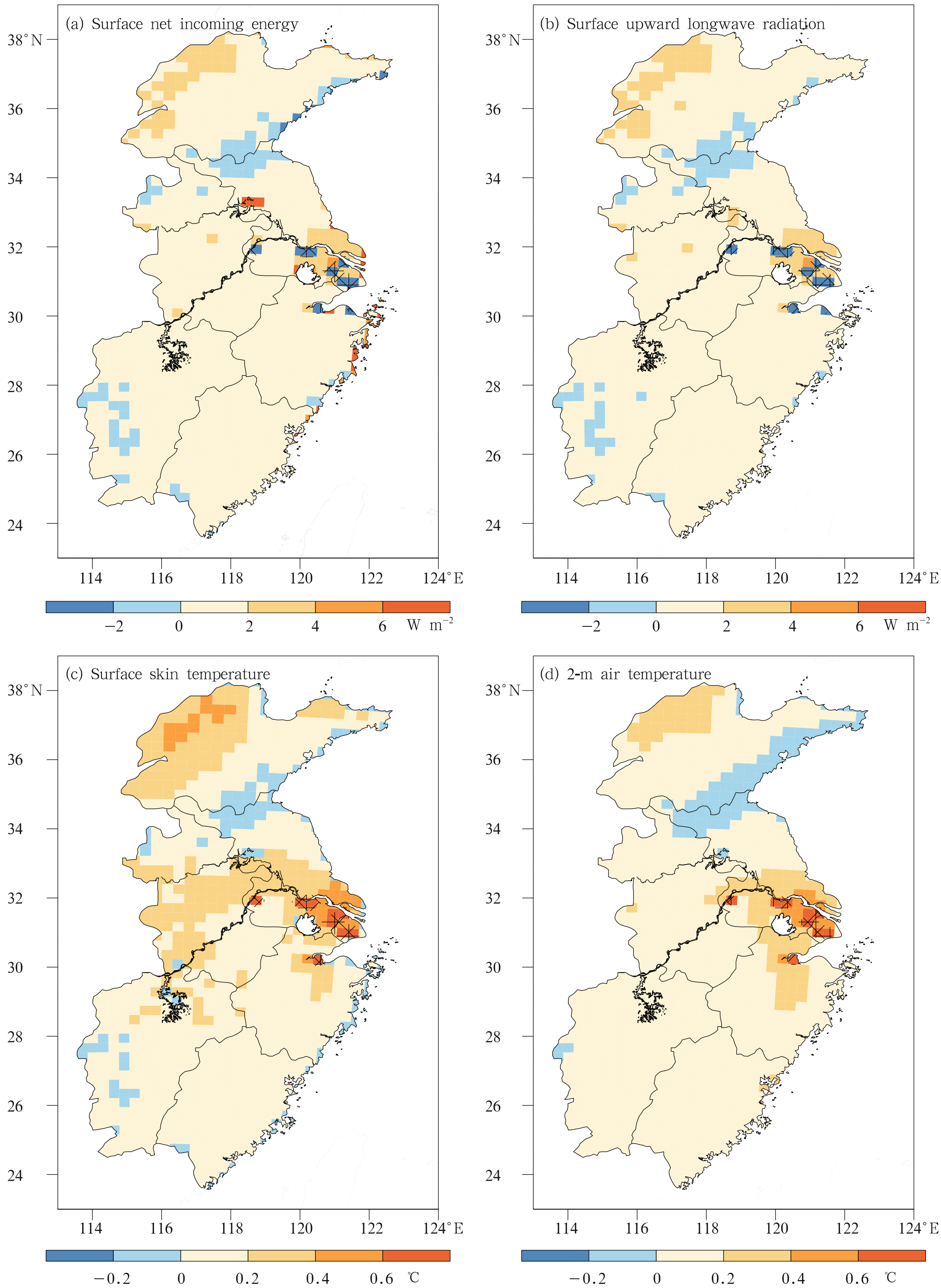


**Fig. 13.** Changes in (a) surface net incoming energy, (b) upward longwave radiation, (c) skin temperature, and (d) 2-m air temperature induced by urban expansion in the YRD during the 2001–2010 Meiyu seasons. Black grids denote those areas in which the change is statistically significant at the 90% confidence level.

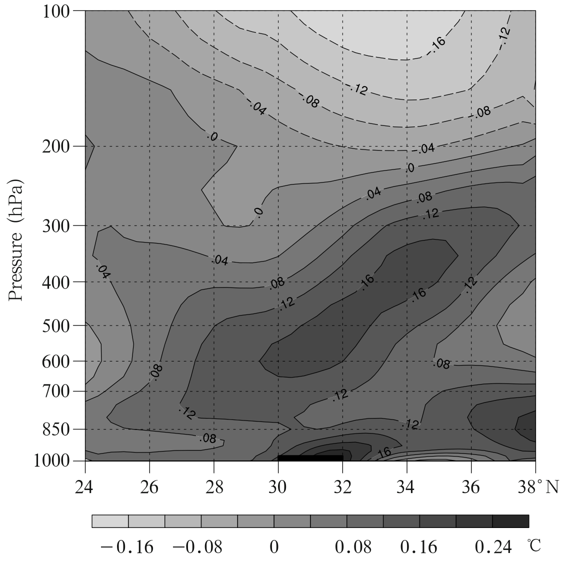


**Fig. 14.** Height-latitude cross-section of air temperature change induced by urban expansion averaged along 115°–122°E during the 2001–2010 Meiyu seasons. The black shading on the bottom indicates the YRD.

M10) were employed to investigate the relationship between the Meiyu precipitation change and urban expansion in the YRD. The following conclusions are drawn.

(1) The WRF model can simulate well the mean distribution, standard deviation of precipitation, and latitudinal-vertical cross-sections of air temperature and pseudo-equivalent temperature during the Meiyu season. The stage characteristics of Meiyu precipitation and the increasing trend of 2-m air temperature can also be well reproduced.

(2) As a result of urban expansion in the YRD, simulated precipitation during the Meiyu period presents an increasing trend (0.2–1.2 mm day$^{-1}$) in the Huaihe River basin and over the land to the south of 28°N, whereas a decreasing trend (0.2–1.2 mm day$^{-1}$) is presented in the Yangtze River basin and over the land to the north of 35°N. Moreover, we find that the spatiotemporal pattern of impact of urban expansion on Meiyu precipitation resembles that of the third EOF mode of the observed precipitation, and this phenomenon suggests a non-negligible relationship between the urban expansion in the YRD and the Meiyu precipitation change in recent years.

(3) Further analyses demonstrate that urban expansion in the YRD changes the surface energy balance over eastern China, which leads to a warming of the 2-m air temperature and tropospheric air temperature, but a cooling of stratospheric air temperature. Furthermore, the increased air temperature leads to a strengthening of the land-sea thermal contrast over eastern China and causes anomalous upward (downward) vertical motion and moisture convergence (divergence) over the Huaihe River (Yangtze River) basin, ultimately leading to the increasing (decreasing) precipitation trend in the Huaihe River (Yangtze River) basin. Therefore, it can be concluded that the warming of tropospheric air temperature and cooling of stratospheric air temperature, which cause the northward shift of the Meiyu belt, can be further strengthened by urban expansion in the YRD. However, it is noted that urban expansion in the YRD causes decreases in surface evaporation, which leads to decreased Meiyu precipitation over the YRD.

However, the reasons why urban expansion affects tropospheric and stratospheric air temperature and leads to their different change patterns have not been investigated. We intend to address this issue in future work. Additionally, the influence of urban expansion in the YRD on regional Meiyu precipitation is extremely complex, because many effects are involved in the process (Zhang et al., 2010). In this paper, we only focus on the physical impacts of urban expansion, including the changes in the surface energy balance, evaporation, air temperature, and regional atmospheric circulation. Previous researchers have found that air pollution (Qian et al., 2009) and the release of waste heat (Feng et al., 2012) can also modify the urban surface energy balance, regional atmospheric circulation, and precipitation. These factors may also need to be considered in future studies to examine the comprehensive impacts of urban expansion on Meiyu precipitation.

***Acknowledgments.*** The authors are very grateful for insightful comments and suggestions by the two anonymous reviewers. We also thank Profs. Huang Anning, Tang Jianping, and Sun Xuguang, as well as Drs. Yang Ben and Xiao Chuliang for their technical support and valuable comments.

## REFERENCES

Bueh, C., Shi Ning, Ji Liren, et al., 2008: Features of the EAP events on the medium-range evolution process and the mid- and high-latitude Rossby wave activities during the Meiyu period. *Chin. Sci. Bull.*, **53**, 610–623.

Bukovsky, M. S., and D. J. Karoly, 2009: Precipitation simulations using WRF as a nested regional climate model. *J. Appl. Meteor. Climate*, **48**, 2152–2159.

Charney, J., W. J. Quirk, S. -H. Chow, et al., 1977: A comparative study of the effects of albedo change on drought in semi-arid regions. *J. Atmos. Sci.*, **34**, 1366–1385.

Chase, T. N., R. A. Pielke, T. G. Kittel, et al., 1996: Sensitivity of a general circulation model to global changes in leaf area index. *J. Geophys. Res.*, **101**, 7393–7408.

Chen, F., and J. Dudhia, 2001: Coupling an advanced land surface-hydrology model with the Penn State-NCAR MM5 modeling system. Part I: Model implementation and sensitivity. *Mon. Wea. Rev.*, **129**, 569–585.

Chen Hong and Xue Feng, 2013: Numerical simulation of decadal variations in the East Asian summer monsoon and summer rainfall in eastern China. *Chinese J. Atmos. Sci.*, **37**, 1143–1153. (in Chinese)

Chen Tsingchang, Wang Shihyu, and Yen Mingcheng, 2007: Enhancement of afternoon thunderstorm activity by urbanization in a valley: Taipei. *J. Appl. Meteor. Climate*, **46**, 1324–1340.

Collins, W. D., P. J. Rasch, B. A. Boville, et al., 2006: The formulation and atmospheric simulation of the Community Atmosphere Model version 3 (CAM3). *J. Climate*, **19**, 2144–2161.

Ding Yihui, Liu Junjie, Sun Ying, et al., 2007: A study of the synoptic-climatology of the Meiyu system in East Asia. *Chinese J. Atmos. Sci.*, **31**, 1082–1101. (in Chinese)

Doll, C. N., 2008: CIESIN Thematic Guide to Night-time Light Remote Sensing and Its Applications. Center for International Earth Science Information Network of Columbia University, Palisades, NY, 19–21.

Du Yin, Xie Zhiqing, Zeng Yan, et al., 2007: Impact of urban expansion on regional temperature change in the Yangtze River Delta. *J. Geogr. Sci.*, **17**, 387–398.

Eastman, J. L., M. B. Coughenour, and R. A. Pielke Sr, 2001: Does grazing affect regional climate? *J. Hydrometeor.*, **2**, 243–253.

Elvidge, C. D., F. -C. Hsu, K. E. Baugh, et al., 2013: National trends in satellite observed lighting: 1992–2012. *Global Urban Monitoring and Assessment through Earth Observation*, Q. Weng, Ed., CRC Press, 2–3.

Feng Jinming, Wang Yongli, Ma Zhuguo, et al., 2012: Simulating the regional impacts of urbanization and anthropogenic heat release on climate across China. *J. Climate*, **25**, 7187–7203.

Foley, J. A., R. DeFries, G. P. Asner, et al., 2005: Global consequences of land use. *Science*, **309**, 570–574.

Ghosh, T., R. L. Powell, C. D. Elvidge, et al., 2010: Shedding light on the global distribution of economic activity. *The Open Geography Journal*, **3**, 148–161.

Gong Daoyi and Ho Changhoi, 2002: Shift in the summer rainfall over the Yangtze River valley in the late 1970s. *Geophys. Res. Lett.*, **29**, 78-1–78-4.

He Chunyang, Shi Peijun, Li Jinggang, et al., 2006: Restoring urbanization process in China in the 1990s by using non-radiance-calibrated DMSP/OLS nighttime light imagery and statistical data. *Chin. Sci. Bull.*, **51**, 1614–1620.

Hong, S. -Y., and J. -O. J. Lim, 2006: The WRF single-moment 6-class microphysics scheme (WSM6). *J. Korean Meteor. Soc.*, **42**, 129–151.

Hong, S. -Y., Y. Noh, and J. Dudhia, 2006: A new vertical diffusion package with an explicit treatment of entrainment processes. *Mon. Wea. Rev.*, **134**, 2318–2341.

Huang Danqing, M. Takahashi, and Zhang Yaocun, 2011: Analysis of the Baiu precipitation and associated circulations simulated by the MIROC Coupled Climate System Model. *J. Meteor. Soc. Japan*, **89**, 625–636.

Jiang Dabang and Wang Huijun, 2005: The natural properties of interdecadal weakening of East Asian summer monsoon in the late of 20th century. *Chin. Sci. Bull.*, **50**, 2256–2262. (in Chinese)

Kain, J. S., 2004: The Kain-Fritsch convective parameterization: An update. *J. Appl. Meteor.*, **43**, 170–181.

Kishtawal, C. M., D. Niyogi, M. Tewari, et al., 2010: Urbanization signature in the observed heavy rainfall climatology over India. *Int. J. Climatol.*, **30**, 1908–1916.

Lin, W. S., C.-H. Sui, L. M. Yang, et al., 2007: A numerical study of the influence of urban expansion on monthly climate in dry autumn over the Pearl River Delta, China. *Theor. Appl. Climatol.*, **89**, 63–72.

Liu Haiwen, Zhou Tianjun, Zhu Yuxiang, et al., 2012: The strengthening East Asian summer monsoon since the early 1990s. *Chin. Sci. Bull.*, **57**, 1553–1558.

Mote, T. L., M. C. Lacke, and J. M. Shepherd, 2007: Radar signatures of the urban effect on precipitation distribution: A case study for Atlanta, Georgia. *Geophys. Res. Lett.*, **34**, L20710, doi: 10.1029/2007GL031903.

Oke, T. R., 1982: The energetic basis of the urban heat island. *Quart. J. Roy. Meteor. Soc.*, **108**, 1–24.

Qian Yun, Gong Daoyi, Fan Jiwen, et al., 2009: Heavy pollution suppresses light rain in China: Observations and modeling. *J. Geophys. Res.*, **114**, doi: 10.1029/2008JD011575.

Ren Guoyu, Zhou Yaqing, Chu Ziying, et al., 2008: Urbanization effects on observed surface air temperature trends in North China. *J. Climate*, **21**, 1333–1348.

Sang, Y. F., Z. Wang, Z. Li, et al., 2013: Investigation into the daily precipitation variability in the Yangtze River Delta, China. *Hydrological Processes*, **27**, 175–185.

Seto, K. C., and J. M. Shepherd, 2009: Global urban land-use trends and climate impacts. *Curr. Opin. Env. Sust.*, **1**, 89–95.

Shepherd, J. M., 2005: A review of current investigations of urban-induced rainfall and recommendations for the future. *Earth Interactions*, **9**, 1–27.

Shepherd, J. M., H. Pierce, and A. J. Negri, 2002: Rainfall modification by major urban areas: Observations from spaceborne rain radar on the TRMM satellite. *J. Appl. Meteor.*, **41**, 689–701.

Shepherd, J. M., M. Carter, M. Manyin, et al., 2010: The impact of urbanization on current and future coastal precipitation: A case study for Houston. *Environment and Planning B: Planning and Design*, **37**, 284–304.

Si Dong, Ding Yihui, and Liu Yanju, 2009: Decadal northward shift of the Meiyu belt and the possible cause. *Chin. Sci. Bull.*, **54**, 4742–4748.

Skamarock, W., J. Klemp, J. Dudhia, et al., 2008: A Description of the Advanced Research WRF Version 3, Mesoscale and Microscale Meteorology Division, National Center For Atmospheric Research, Boulder, Colorado, 1–2.

Small, C., F. Pozzi, and C. D. Elvidge, 2005: Spatial analysis of global urban extent from DMSP-OLS night lights. *Remote Sens. Environ.*, **96**, 277–291.

Stohlgren, T. J., T. N. Chase, R. A. Pielke, et al., 1998: Evidence that local land use practices influence regional climate, vegetation, and stream flow patterns in adjacent natural areas. *Global Change Biology*, **4**, 495–504.

Su, Z., 2002: The Surface Energy Balance System (SEBS) for estimation of turbulent heat fluxes. *Hydrology and Earth System Sciences*, **6**, 85–99.

Wan Hongchao, Zhong Zhong, Yang Xiuqun, et al., 2013: Impact of city belt in Yangtze River Delta in China on a precipitation process in summer: A case study. *Atmos. Res.*, 125-126, 63–75.

Wang Huijun, 2001: The weakening of the Asian monsoon circulation after the end of 1970's. *Adv. Atmos. Sci.*, **18**, 376–386.

Wang Jun, Feng Jinming, Yan Zhongwei, et al., 2012: Nested high-resolution modeling of the impact of urbanization on regional climate in three vast urban agglomerations in China. *J. Geophys. Res.*, **117**, doi: 10.1029/2012JD018226.

Wei Fengying and Xie Yu, 2005: Interannual and interdecadal oscillations of Meiyu over the middle lower reaches of the Chang-Jiang River for 1885–2000. *J. Appl. Meteor. Sci.*, **16**, 492–499. (in Chinese)

Wu Kai and Yang Xiuqun, 2013: Urbanization and heterogeneous surface warming in eastern China. *Chin. Sci. Bull.*, **58**, 1363–1373, doi: 10.1007/s11434-012-5627-8.

Wu Rong and Zhang Yaocun, 2012: Performance of RegCM3 in simulating the rainfall and associated circulation in Meiyu period of Yangtze and Huaihe River valleys. *J. Meteor. Sci.*, **32**, 119–126. (in Chinese)

Xue, Y. K., H. M. H. Juang, W. P. Li, et al., 2004: Role of land surface processes in monsoon development: East Asia and West Africa. *J. Geophys. Res.*, **109**, D03105, doi: 10.1029/2003JD003556.

Yang Ben, Zhang Yaocun, and Qian Yun, 2012: Simulation of urban climate with high-resolution WRF model: A case study in Nanjing, China. *Asia-Pacific J. Atmos. Sci.*, **48**, 227–241, doi: 10.1007/s13143-012-0023-5.

Yang Xuchao, Hou Yiling, and Chen Baode, 2011: Observed surface warming induced by urbanization in East China. *J. Geophys. Res.*, **116**, doi: 10.1029/2010JD015452.

Yu Rucong, Wang Bin, and Zhou Tianjun, 2004: Tropospheric cooling and summer monsoon weakening trend over East Asia. *Geophys. Res. Lett.*, **31**, doi: 10.1029/2004GL021270.

Zhang Chaolin, Chen Fei, Miao Shiguang, et al., 2009: Impacts of urban expansion and future green planting on summer precipitation in the Beijing metropolitan area. *J. Geophys. Res.*, **114**, doi: 10.1029/2008JD010328.

Zhang Jiao, Wang Dongyong, Tian Hong, et al., 2008: Comparative analysis of atmospheric circulation characteristic over Huaihe River during the severe precipitation between 2003 and 2005. *Scientia Meteor. Sinica*, **28**, 402–408. (in Chinese)

Zhang Jingyong, Wu Lingyun, and Dong Wenjie, 2011: Land-atmosphere coupling and summer climate variability over East Asia. *J. Geophys. Res.*, **116**, doi: 10.1029/2010JD014714.

Zhang Ning, Gao Zhiqiu, Wang Xuemei, et al., 2010: Modeling the impact of urbanization on the local and regional climate in Yangtze River Delta, China. *Theor. Appl. Climatol.*, **102**, 331–342.

Zhao Linna, Yang Xiaodan, Qi Dan, et al., 2007: The analysis of precipitation and flooding features in the Huaihe River basin during the summer of 2007. *Climatic Environ. Res.*, **12**, 728–737. (in Chinese)

Zong Haifeng, Zhang Qingyun, and Chen Lieting, 2006: Temporal and spatial variations of precipitation in eastern China during the Meiyu period and their relationships with circulation and sea surface temperature. *Chinese J. Atmos. Sci.*, **30**, 1189–1197. (in Chinese)